Journal of Materials Chemistry C

Dynamic Article Links ►

Cite this: DOI: 10.1039/c0xx00000x

ARTICLE TYPE

www.rsc.org/xxxxxx

Phthalocyanine-based Discotic Liquid Crystal Switching from Molten Alkyl Chain Type to Flying-seed-like Type

Hiromu Nakamura,[a] Kouki Sugiyama,[a] Kazuchika Ohta*[a] and Mikio Yasutake[b]

Received (in XXX, XXX) Xth XXXXXXXXX 20XX, Accepted Xth XXXXXXXXX 20XX

DOI: 10.1039/b000000x

We have synthesised a series of the phthalocyanine-based discotic liquid crystals, (*m*-C_nOPhO)$_8$PcCu (*n* = 1-20: **2a-o**), and investigated their mesomorphism by using a polarizing optical microscopy (POM), a differential scanning calorimeter (DSC) and a temperature-dependent small angle X-ray diffractometer. We found that each of the derivatives **2a-o** shows mesomorphism. However, the mesomorphism of the (*m*-C_nOPhO)$_8$PcCu derivatives strongly depends on the alkoxy chain length (*n*). The mesomorphism of the short chain-substituted derivatives **2a-e** for n = 1~5 is flying-seed-like type induced by flip-flop of the peripheral bulky substituents, whereas the mesomorphism of the long chain-substituted derivatives **2j-o** for n = 10~20 is conventional molten alkyl chain type induced by melting of the long alkyl chains. The moderately long chain derivatives (**2f-i**) for *n* = 6-9 in between show both types of mesophases. The detailed temperature-dependent X-ray diffraction measurements were carried out for three representative derivatives, **2b** (*n* = 2 for *n* = 1-5), **2h** (*n* = 8 for *n* = 6-9), and **2o** (*n* = 20 for *n* = 10-20). As a result, we revealed that the Col_{ro}(P2m) mesophase in **2b** (*n* = 2) gave a halo denoted as **Halo$_{arom.}$** at d ≅ 5.2 Å due to flip-flop of the bulky aromatic substituents, and that the Col_{ho} mesophase in **2o** (n = 20) gave a halo denoted as **Halo$_{alkyl}$** at d ≅ 4.6-4.8 Å due to melting of the long alkyl chains. Therefore, we can distinguish the type of mesophase from **Halo$_{arom.}$** and **Halo$_{alkyl}$**. Very interestingly, the (*m*-C_8OPhO)$_8$PcCu (**2h**) derivative having moderately long alkyl chains gave **Halo$_{alkyl}$** at about 4.8 Å in the lower temperature mesophase of Col_{ho}, but **Halo$_{arom}$** at about 5.2 Å in the higher temperature mesophase of Col_{ro}($P2_1/a$) phase. This means that melting of the alkyl chains induces the Col_{ho} phase in the lower temperature region, but that flip-flop of the bulky aromatic substituents induces the Col_{ro}($P2_1/a$) phase in the higher temperature region. This unusual reverse phase transition sequence from a higher symmetry of Col_h mesophase to a lower symmetry of Col_r mesophase on heating stage is attributable to such a unique stepwise melting of these two different types of substituents. To our best knowledge, this mesogen (**2h**) is the first example switching mesomorphism from molten alkyl chain type to flying-seed-like type in a discotic liquid crystal.

1. INTRODUCTION

Since the first liquid crystalline compounds were discovered by Reinitzer[1] in 1888, over 100,000 kinds of liquid crystalline compounds[2] have been synthesised up to date. These liquid crystalline compounds are generally classified into rod-like molecules and discotic molecules judging from their molecular shapes, but both of them commonly have a structure having a rigid core at the centre and several flexible long alkyl chains in the periphery. When these liquid crystalline compounds are heated, the long alkyl chains melt at first to form a soft part, whereas the central cores remain as a rigid part without melting, so that mesomorphism can be induced. Therefore, until now, we have long believed that it is essential for a liquid crystalline molecule to have a rigid core in the centre and flexible long alkyl chains in the periphery. However, it has been reported that a very few liquid crystalline compounds have neither a rigid core in the centre nor flexible long alkyl chains in the periphery.[3-11]

In 1911, Vorländer reported that sodium diphenylacetate, potassium dimethylacetate and potassium diethylacetate show mesomorphism although there is neither a rigid core in the centre nor flexible long alkyl chains in the periphery.[3] However, he only reported that they show mesophases, but that neither their mesophase identification nor the mesomorphism induction mechanism was clarified. In the past 100 years, a very few researchers, Demus,[4] Sanesi,[5, 6] Binnnemans,[7] and our group,[8] have investigated these liquid crystalline compounds. In 2006, we clarified the mesomorphism induction mechanism of sodium diphenylacetate, potassium dimethylacetate and potassium diethylacetate by using temperature-dependent X-ray diffractometer.[8]

Sodium diphenylacetate shows a hexagonal columnar (Col_h) phase. On the other hand, potassium dimethylacetate and potassium diethylacetate show a smectic A (SmA) phase. These compounds form a soft part by free rotation of the bulky substituents, diphenylmethyl, dimethylmethyl and diethylmethyl groups. Sodium metals form a one-dimensional nano-wire and diphenylmethyl groups freely rotate around the nano-wire to form an aromatic nanotube, so that sodium diphenylacetate shows a Col_h phase. On the other hand, in potassium dimethylacetate and potassium diethylacetate, potassium metals form a two-dimensional potassium metal sheet and dimethylmethyl or diethylmethyl groups freely rotate to form an aliphatic sheet, so that they show a SmA phase. Such unique mesomorphism induction mechanism has never been reported so far. Since the freely rotating substituents very resemble flying seeds of a maple tree, we named such type of liquid crystals as **flying-seed-like liquid crystals**.[8]

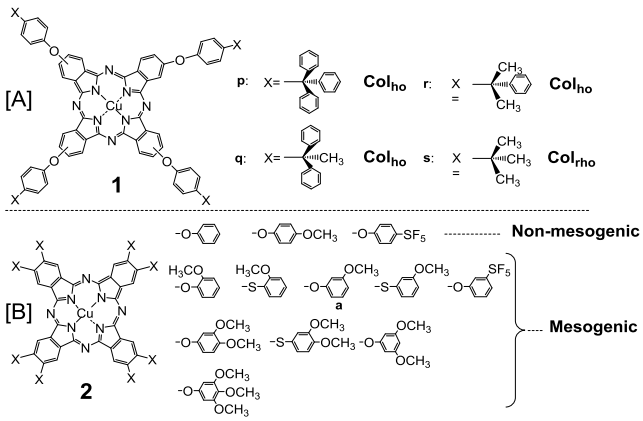

Fig. 1 Flying-seed-like liquid crystals based on phthalocyanine: [A] the first flying-seed-like liquid crystals, **1p~s**, based on phthalocyanine.[12-14]; [B] dependence of liquid crystallinity on the substitution position for phthalocyanine-based compounds, **2**.[16-18]

In 2009, Usol'tseva *et al.*, reported a phthalocyanine derivative (**1p** in Figure 1A) substituted by four *p*-(triphenylmethyl)phenoxy groups shows a Col_h phase, although it has no long alkyl chains in the periphery.[12, 13] In their reports, the mesophase was identified only by polarizing microscopic observation (POM), without the X-ray diffraction measurement. In 2012, we therefore synthesised a series of phthalocyanine homologues (**1p-s**) shown in Figure 1A,[14] in order to investigate the detailed phase structures of these compounds by the temperature-dependent X-ray diffraction measurements. As a result, we established that the homologue **1p** shows a Col_{ho} phase as reported by Usol'tseva *et al.* The phthalocyanine homologues **1q-r** also show the same Col_{ho} phase, whereas the homologue **1s** only shows a pseudohexagonal ordered columnar (Col_{rho}) phase.[14] Generally, liquid crystalline phases give a halo observed at *ca.*4.5 Å due to melting of the long alkyl chains. However, the present phthalocyanine homologues **1p-s** gave an alternative halo at 5.7 Å ~ 6.9 Å due to free rotation of the bulky substituents. It was confirmed from these phthalocyanine homologues (**1p-s**) that introduction of bulky substituents instead of long alkyl chains into the periphery of a rigid core can also induce mesomorphism.

In the past five years, we have explored several novel flying-seed-like liquid crystals.[14-19] Figure 1B shows our developed flying-seed-like phthalocyanine derivatives substituted by bulky substituents to induce mesomorphism. As can be seen from this figure, the non-substituted phenoxy group, the *p*-methoxyphenoxy group and *p*-pentafluorosulfanylphenoxy group cannot induce mesomorphism.[17, 18] On the other hand, the compounds having a methoxy group at the *ortho* position or the *meta* position show mesomorphism.[17] Interestingly, when a methoxy group is introduced at least at the *meta* position in the phenoxy group, these compounds tend to show mesomorphism.[17] When a phenoxy group is replaced by a phenylthio group, the compounds substituted by a methoxy group at the *ortho* and *meta* positions in the phenylthio also show mesomorphism.[16] This tendency could be seen also for the pentafluorosulfanyl substituted homologue.[18] Thus, the introduction of the substituent at the *m*-position can induce the flying-seed-like mesomorphism. This means that rotation or flip-flop of the *m*-methoxyphenoxy groups may originate the large exclusion volume to form a soft part necessary to induce mesomorphism.[17]

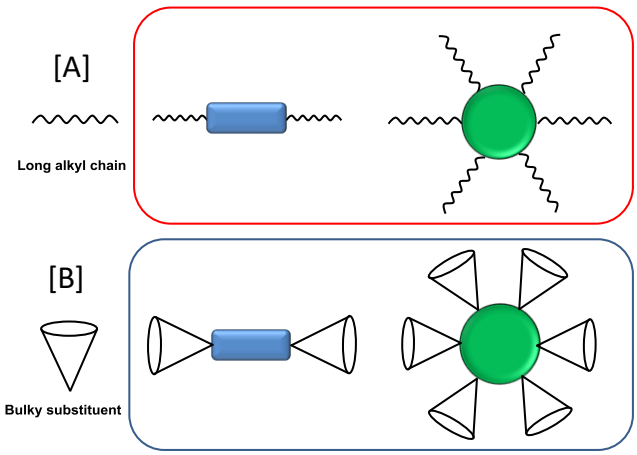

Fig. 2 Variety of liquid crystalline compounds: [A] conventional molten alkyl chain type of liquid crystals originated from melting of the long alkyl chains in the periphery, and [B] flying-seed-like liquid crystals originated from free rotation of the bulky substituents in the periphery.

Therefore, mesomorphism can be induced from two different types, as illustrated in Figure 2: [A] melting of the long alkyl chains in the periphery to induce conventional molten alkyl chain type of liquid crystals, and [B] free rotation or flip-flop of the bulky substituents in the periphery to induce novel flying-seed-like liquid crystals.

Hereupon, we focused on the phthalocyanine derivative (m-C_1OPhO)$_8$PcCu (**2a** in Figure 1) showing columnar mesomorphism. In this derivative (**2a** in Figure 3A), a very short methoxy group is substituted at the *meta* position of the phenoxy group. On the other hand, the homologous phthalocyanine derivative substituted by a long eicosanyloxy group at the *meta* position of the phenoxy group (m-C_nOPhO)$_8$PcCu (n = 20: **2o** in Figure 3B) also show columnar mesomorphism, as previously reported.[20, 21] The flying-seed-like mesomorphism of the (m-C_1OPhO)$_8$PcCu (**2a**) derivative may be induced by flip-flop of the peripheral bulky substituents, as shown in Figure 3A, whereas the mesomorphism of the (m-C_{20}OPhO)$_8$PcCu (**2o**) derivative

may be induced by melting of the long alkyl chains like conventional liquid crystals, as shown in Figure 3B. Hence, mesomorphism of these two derivatives, **2a** and **2o**, may be induced from different driving forces. If we will synthesise a series of the (*m*-C_nOPhO)$_8$PcCu derivatives for n = 1-20 to investigate their mesomorphism, we will be able to reveal the boundary of mesomorphism inducing driving forces switching from flying-seed-like type to molten alkyl chain type in the alkyl chain length, n = 1~ 20.

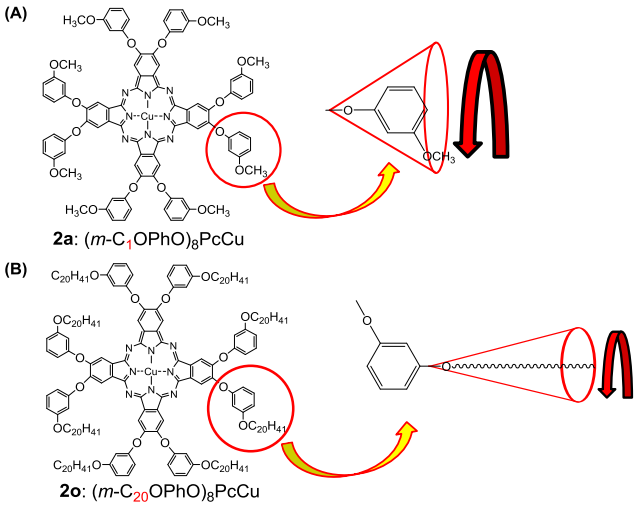

Fig. 3 Molecular formulae of liquid crystals based on phthalocyanine in our previous works: (A) flying-seed-like type liquid crystal, **2a**, and (B) molten alkyl chain type liquid crystal, **2o**.

In this study, we have therefore synthesised additional homologues of (*m*-C_nOPhO)$_8$PcCu (*n* = 2-9: **2b-i** in Scheme 1) to investigate the boundary of the alkyl chain length in a series of the homologues **2a-o** (*n* = 1~ 20). To our best knowledge, such a unique research has never been done up to date.

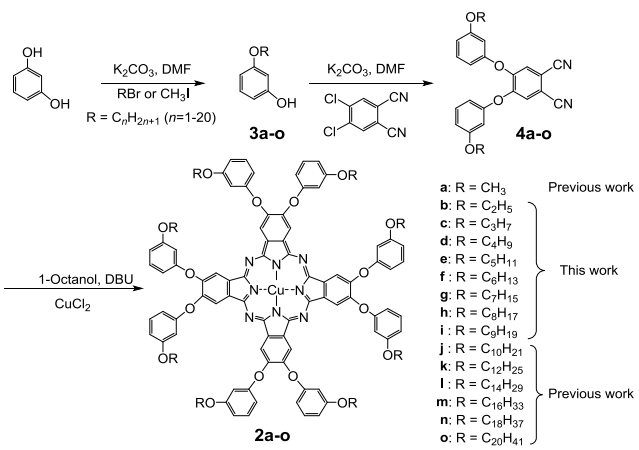

Scheme 1 Synthetic route for (*m*-C_nOPhO)$_8$PcCu (n = 1-20: **2a-o**), DMF = N,N'-dimethylformamide and DBU = 1,8-diazabicyclo[5,4,0]-undec-7-ene. **a** = Ref. 17, **k**, **l** = Ref. 20 and **j**, **m-o** = Ref. 21.

2. EXPERIMENTAL

2-1. Synthesis

Scheme 1 shows synthetic route for octakis(*m*-*n*-alkoxyphenoxy)phthalocyaninato copper(II) (*m*-C_nOPhO)$_8$PcCu (*n*=2-9: **2b-i**). The synthesis was adopted our previously reported methods.[20, 21] Phenol derivatives (**3b-i**) were synthesised by Williamson ether synthesis with resorcinol and the corresponding 1-bromoalkane purchased from Wako Pure Chemical Industries, Ltd. Phthalonitrile derivatives (**4b-i**) were synthesised by aromatic substitution with phenol derivatives (**3b-i**) and 4,5-dichlorophthalonitrile purchased from Tokyo Chemical Industry (Tokyo Kasei). The target phthalocyanine derivatives (**2b-i**) were synthesised by cyclic tetramerization of the corresponding dicyano compounds (**3b-i**).

The detailed procedures are described below only for a representative compound, (*m*-C_2OPhO)$_8$PcCu (**2b**).

3-Ethoxyphenol (3b)

A mixture of resorcinol (4.00 g, 36.4 mmol), K_2CO_3 (1.49 g, 10.8 mmol) and dry DMF (12.5 mL) was stirred at 70°C under the nitrogen atmosphere for 25 min. Then, bromoethane (5.13 g, 47.1 mmol) was added to the mixture and it was stirred at 95°C under the nitrogen atmosphere for 3 h 50 min. The reaction mixture was extracted with chloroform and washed with water. The organic layer was dried over Na_2SO_4 for 1h. After removing the Na_2SO_4 by filtration, the filtrate was evaporated in *vacuum* using an evaporator. The residue was purified by column chromatography (silica gel, chloroform, R_f = 0.25) to obtain 0.276 g of reddish brown liquid. Yield = 55.3 %. ^{1}H NMR (400 MH$_Z$; $CDCl_3$; Me_4Si): δ (ppm) = 1.39 (3 H, t, J = 7.2 H$_Z$, -CH_3), 4.00 (2 H, q, J = 6.9 H$_Z$, -OCH_2-), 5.72 (1 H, s, Ar-OH), 6.41-6.44 (2 H, m, Ar-H), 6.45-6.48 (1 H, m, Ar-H) and 7.10 (1 H, t, J = 8.4 H$_Z$, Ar-H).

Since other homologues (**3c-i**) were synthesised in the same way, only the yields and ^{1}H-NMR data are described below.

3-Propoxyphenol (3c)

Yield = 34.5 %. Liquid at rt. ^{1}H NMR (400 MH$_Z$; DMSO; Me_4Si): δ (ppm) = 0.96 (3 H, t, J = 7.4 H$_Z$, -CH_3), 1.70 (2 H, sext., J =7.0 H$_Z$, -CH_2-), 3.84 (2 H, t, J = 6.6H$_Z$, -OCH_2-), 6.31-6.36 (3 H, m, Ar-H), 7.03 (1 H, t, J = 8.0 H$_Z$, Ar-H) and 9.35 (1 H, s, Ar-OH).

3-Buthoxyphenol (3d)

Yield = 35.7 %. Liquid at rt. ^{1}H NMR (400 MH$_Z$; $CDCl_3$; Me_4Si): δ (ppm) = 0.90 (3 H, t, J = 7.4 Hz, -CH_3), 1.41 (2 H, sext., J = 7.6 Hz, -CH_2-), 1.68 (2 H, quin., J = 6.1 Hz, -CH_2-), 3.86 (2 H, t, J = 6.8 Hz, -OCH_2-), 4.99 (1 H, s, Ar-OH), 6.32-6.35 (2 H, m, Ar-H), 6.40-6.42 (1 H, m, Ar-H) and 7.04 (1 H, t, J = 8.4 Hz, Ar-H).

3-Pentyloxyphenol (3e)

Yield = 20.5 %. Liquid at rt. ^{1}H NMR (400 MH$_Z$; $CDCl_3$; Me_4Si): δ (ppm) = 0.96 (3 H, t, J = 7.1 H$_Z$, -CH_3), 1.36-1.49 (4 H, m, -C_2H_4-), 1.80 (2 H, quin., J = 7.0 H$_Z$, -CH_2-), 3.95 (2 H, t, J = 6.6 H$_Z$, -OCH_2-), 5.40 (1 H, s, Ar-OH), 6.43-6.46 (2 H, m, Ar-H), 6.50-6.53 (1 H, m, Ar-H) and 7.14 (1 H, t, J = 8.6 Hz, Ar-H).

3-Heptyloxyphenol (3g)

Yield = 18.5 %. Liquid at rt. ^{1}H NMR (400 MH$_Z$; $CDCl_3$; Me_4Si): δ (ppm) = 0.93 (3 H, t, J = 7.0 H$_Z$, -CH_3), 1.30-1.50 (8 H, m, -C_4H_8-), 1.79 (2 H, quin., J = 7.0 H$_Z$, -CH_2-), 3.94 (2 H, t, J = 6.6 H$_Z$, -OCH_2-), 5.34 (1 H, s, Ar-OH), 6.43-6.46 (2 H, m, Ar-H), 6.50-6.53 (1 H, m, Ar-H) and 7.14 (1 H, t, J = 8.4 Hz, Ar-H).

3-Octyloxyphenol (3h)

Yield = 48.3 %. Liquid at rt. ^{1}H NMR (400 MH$_Z$; $CDCl_3$; Me_4Si): δ (ppm) = 0.91 (3 H, t, J = 7.0 H$_Z$, -CH_3), 1.31-1.50 (8 H, m,

-C_5H_{10}-), 1.79 (2 H, quin., J = 7.0 H_z, -CH_2-), 3.95 (2 H, t, J = 6.6 H_z, -OCH_2-), 5.40 (1 H, s, Ar-OH), 6.43-6.46 (2 H, m, Ar-H), 6.50-6.53 (1 H, m, Ar-H) and 7.14 (1 H, t, J = 8.4 Hz, Ar-H).

3-Nonyloxyphenol (3i)

Yield = 16.3 %. Liquid at rt. ^{1}H NMR (400 MH_z; $CDCl_3$; Me_4Si): δ (ppm) = 0.92 (3 H, t, J = 6.8 H_z, -CH_3), 1.27-1.50 (12 H, m, -C_6H_{12}-), 1.79 (2 H, quin., J = 7.2 H_z, -CH_2-), 3.94 (2 H, t, J = 6.6 H_z, -OCH_2-), 5.07 (1 H, s, Ar-OH), 6.42-6.45 (2 H, m, Ar-H), 6.50-6.53 (1 H, m, Ar-H) and 7.14 (1 H, t, J = 8.4 Hz, Ar-H).

4,5-Bis(3-ethoxyphenoxy)phthalonitrile (4b)

A mixture of 3-ethoxyphenol (**3b**) (0.624 g, 4.52 mmol), K_2CO_3 (0.632 g, 4.57 mmol) and dry DMF (30 mL) was stirred at 90°C under the nitrogen atmosphere for 10 min. Then, 4,5-dichlorophtalonitrile (0.394 g, 2.00 mmol) was added to the mixture and it was stirred at 100°C under the nitrogen atmosphere for 1 h 50 min. The reaction mixture was extracted with chloroform and washed with water. The organic layer was dried over Na_2SO_4 for 1h. After removing the Na_2SO_4 by filtration, the filtrate was evaporated in *vacuum* using an evaporator. The residue was purified by column chromatography (silica gel, toluene, R_f = 0.25) to obtain 0.423 g of light blue solid. Yield = 51.5 %. M.p. = 125.0~125.4°C. ^{1}H NMR (400 MH_z; $CDCl_3$; Me_4Si): δ (ppm) = 1.37 (6 H, t, J = 7.0 H_z, -CH_3), 3.78 (4 H, q, J = 6.9 H_z, -OCH_2-), 6.53-6.58 (4 H, m, Ar-H), 6.79-6.81 (2 H, m, Ar-H), 7.04 (2 H, s, Ar-H) and 7.30 (2 H, t, J = 8.2 H_z, Ar-H). IR: (KBr, ν_{max} / cm^{-1}) 2241 (-CN).

Since other homologues (**4c-i**) were synthesised in the same way, only the yields, ^{1}H-NMR data and FT-IR data are described below.

4,5-Bis(3-propooxyphenoxy)phthalonitrile (4c)

Yield = 86.1 %. M.p. = 38.0~38.5°C. ^{1}H NMR (400 MH_Z; $CDCl_3$; Me_4Si): δ (ppm) = 1.07 (6 H, t, J = 7.2 Hz, -CH_3), 1.84 (4 H, sext, J = 7.0 Hz, -CH_2-), 3.95 (4 H, t, J = 6.6 Hz, -OCH_2-), 6.63-6.67 (4 H, m, Ar-H), 6.83-6.86 (2 H, m, Ar-H), 7.22 (1 H, s, Ar-H) and 7.35 (2 H, t, J = 8.2 Hz, Ar-H). IR: (KBr, ν_{max} / cm^{-1}) 2238 (-CN).

4,5-Bis(3-buthoxyphenoxy)phthalonitrile (4d)

Yield = 19.5 %. Liquid at rt. ^{1}H NMR (400 MH_Z; $CDCl_3$; Me_4Si): δ (ppm) = 1.00 (6 H, t, J = 7.4 Hz, -CH_3), 1.52 (4H, sext., J = 7.6 Hz, -CH_2-), 1.80 (4 H, quin., J = 6.0 Hz, -CH_2-), 3.98 (4 H, t, J = 6.4 Hz, -OCH_2-), 6.63-6.67 (4 H, m, Ar-H), 6.82-6.85 (2 H, m, Ar-H), 7.23 (1 H, s, Ar-H) and 7.34 (2 H, t, J = 8.2 Hz, Ar-H). IR: (KBr, ν_{max} / cm^{-1}) 2233 (-CN).

4,5-Bis(3-pentyloxyphenoxy)phthalonitrile (4e)

Yield = 73.4 %. Liquid at rt. ^{1}H NMR (400 MH_z; $CDCl_3$; Me_4Si): δ (ppm) = 0.86 (6 H, t, J = 7.0 H_z, -CH_3), 1.27-1.41 (8 H, m, -C_2H_4-), 1.72 (4 H, quin., J = 7.0 Hz, -C_2H_4-), 3.88 (4 H, t, J = 6.6 H_z, -OCH_2-), 6.53-6.57 (4 H, m, Ar-H), 6.72-6.75 (2 H, m, Ar-H), 7.13(2 H, s, Ar-H) and 7.25 (2 H, t, J = 8.0 Hz, Ar-H). IR: (KBr, ν_{max} / cm^{-1}); 2233 (-CN).

4,5-Bis(3-heptyloxyphenoxy)phthalonitrile (4g)

Yield = 98.7 %. Liquid at rt. ^{1}H NMR (400 MH_z; $CDCl_3$; Me_4Si): δ (ppm) = 0.82 (6 H, t, J = 6.8 H_z, -CH_3), 1.19-1.42 (16 H, m, -C_4H_8-), 1.72 (4 H, quin., J = 7.0 Hz, -CH_2-), 3.88 (4 H, t, J = 6.4 H_z, -OCH_2-), 6.53-6.57 (4 H, m, Ar-H), 6.72-6.75 (2 H, m, Ar-H), 7.13(2 H, s, Ar-H) and 7.25 (2H, t, J = 8.4 Hz, Ar-H). IR: (KBr, ν_{max} / cm^{-1}) 2233 (-CN).

4,5-Bis(3-octyloxyphenoxy)phthalonitrile (4h)

Yield = 75.9 %. Liquid at rt. ^{1}H NMR (400 MH_z; $CDCl_3$; Me_4Si): δ (ppm) = 0.82 (6 H, t, J = 7.0 H_z, -CH_3), 1.21-1.42 (16 H, m, -C_5H_{10}-), 1.72 (4 H, quin., J = 7.0 Hz, -CH_2-), 3.88 (4 H, t, J = 6.6 H_z, -OCH_2-), 6.53-6.57 (4 H, m, Ar-H), 6.73-6.75 (2 H, m, Ar-H), 7.13(2 H, s, Ar-H) and 7.25 (2 H, t, J = 8.4 Hz, Ar-H). IR: (KBr, ν_{max} / cm^{-1}) 2233 (-CN).

4,5-Bis(3-nonyloxyphenoxy)phthalonitrile (4i)

Yield = 75.9 %. M.p. = 38.0~38.5°C. ^{1}H NMR (400 MH_z; $CDCl_3$; Me_4Si): δ (ppm) = 0.81 (6 H, t, J = 6.8 H_z, -CH_3) 1.20-1.42 (20 H, m, -C_6H_{12}-), 1.71 (4 H, quin., J = 7.0 Hz, -C_2H_4-), 3.87 (4 H, t, J = 6.6 H_z, -OCH_2-), 6.53-6.57 (4 H, m, Ar-H), 6.72-6.75 (2 H, m, Ar-H), 7.13(2 H, s, Ar-H) and 7.25 (2 H, t, J = 8.0 Hz, Ar-H). IR: (KBr, ν_{max} / cm^{-1}) 2237 (-CN).

(*m*-C_2OPhO)$_8$PcCu (2b)

A mixture of 4,5-bis(3-ethoxyphenoxy)phthalonitrile (**4b**) (0.201 g, 0.502 mmol), 1-octatanol (5 mL), $CuCl_2$ (0.022 g、0.162 mmol) and DBU (4 drops) was refluxed under the nitrogen atmosphere for 3 h 10 min. Methanol was poured into the reaction mixture to precipitate the target compound. The methanolic layer was removed by filtration and then resulting precipitate was washed with methanol, ethanol and acetone, respectively. The residue was purified by hot filtration with chloroform to obtain 0.137 g of green solid. Yield = 65.3 %.

Yields, elemental analysis data and MALDI-TOF mass data: See Table 1.UV-vis spectral data: See Table 2.

The other homologues (**2c-i**) could be similarly synthesised. The yields, elemental analysis data and MALDI-TOF mass data are shown in Table 1 and the UV-Vis spectrum data are summarized in Table 2.

Table 1. TOF-Mass spectral data, elemental analysis data and yields of (*m*-C_nOPhO)$_8$PcCu (n=2-9: **2b-i**).

Compound	Mol. formula (Mol. wt)	Exact mass		Elemental analysis: Found(Calcd.)(%)			Yield(%)
		Calcd.	Observed	C	H	N	
2b: (*m*-C_2OPhO)$_8$PcCu	$C_{96}H_{80}CuN_8O_{16}$ (1665.25)	1663.32	1663.32	69.30 (69.24)	5.00 (4.84)	7.05 (6.73)	65.3
2c: (*m*-C_3OPhO)$_8$PcCu	$C_{104}H_{96}CuN_8O_{16}$ (1777.47)	1775.62	1775.49	70.44 (70.27)	5.63 (5.44)	6.42 (6.30)	59.9
2d: (*m*-C_4OPhO)$_8$PcCu	$C_{112}H_{112}CuN_8O_{16}$ (1889.68)	1887.75	1887.56	71.09 (71.19)	5.93 (5.97)	6.18 (5.93)	69.9
2e: (*m*-C_5OPhO)$_8$PcCu	$C_{120}H_{128}CuN_8O_{16}$ (2001.89)	1999.88	1999.63	72.00 (72.13)	6.44 (6.74)	5.60 (5.78)	47.4
2f: (*m*-C_6OPhO)$_8$PcCu	$C_{128}H_{144}CuN_8O_{16}$ (2114.10)	2112.01	2112.07	72.72 (72.59)	6.87 (7.05)	5.30 (5.29)	55.9
2g: (*m*-C_7OPhO)$_8$PcCu	$C_{136}H_{160}CuN_8O_{16}$ (2226.32)	2224.13	2223.95	73.37 (73.31)	7.24 (7.47)	5.03 (5.36)	58.7
2h: (*m*-C_8OPhO)$_8$PcCu	$C_{144}H_{176}CuN_8O_{16}$ (2338.53)	2336.26	2336.36	73.96 (73.74)	7.59 (7.75)	4.79 (4.65)	44.7
2i: (*m*-C_9OPhO)$_8$PcCu	$C_{152}H_{192}CuN_8O_{16}$ (2450.74)	2448.39	2448.27	74.49 (74.73)	7.90 (8.05)	4.57 (4.60)	43.1

Table 2. UV-vis spectral data in chloroform of (*m*-C_nOPhO)$_8$PcCu (n=3-9: **2c-i**).

Compound	Concentration[b] (X10^{-6}mol/L)	λ_{max} (nm) (log ε)					
		Soret-band			Q-band		
					$Q_{0\text{-}1}$-band	*	$Q_{0\text{-}0}$-band
2b:(*m*-C_2OPhO)$_8$PcCu[a]	-	-	-	-	-	-	-
2c:(*m*-C_3OPhO)$_8$PcCu	3.45	283.2(4.83)	342.2(4.91)	*ca.*383(4.54)[φ]	613.8(4.63)	*ca.*652(4.59)[o]	682.4(5.33)
2d:(*m*-C_4OPhO)$_8$PcCu	3.45	282.5(4.84)	340.4(4.92)	*ca.*383(4.55)[φ]	614.5(4.68)	*ca.*651(4.66)[o]	682.1(5.42)
2e:(*m*-C_5OPhO)$_8$PcCu	3.46	283.7(4.82)	343.9(4.90)	*ca.*382(4.53)[φ]	614.9(4.65)	*ca.*651(4.63)[o]	681.8(5.39)
2f:(*m*-C_6OPhO)$_8$PcCu	3.46	283.9(4.87)	341.0(4.94)	*ca.*382(4.57)[φ]	613.5(4.69)	*ca.*652(4.67)[o]	681.9(5.43)
2g:(*m*-C_7OPhO)$_8$PcCu	3.45	283.8(4.87)	339.5(4.95)	*ca.*383(4.57)[φ]	613.1(4.70)	*ca.*654(4.66)[o]	681.8(5.43)
2h:(*m*-C_8OPhO)$_8$PcCu	3.46	283.7(4.88)	342.1(4.94)	*ca.*382(4.56)[φ]	613.6(4.69)	*ca.*652(4.67)[o]	680.9(5.43)
2i:(*m*-C_9OPhO)$_8$PcCu	3.44	283.8(4.90)	342.6(4.97)	*ca.*382(4.59)[φ]	612.9(4.73)	*ca.*653(4.69)[o]	681.6(5.46)

[a]: This derivative was insoluble in all the solvents. [b]: In chloroform. *: Aggregation band of $Q_{0\text{-}0}$-band. [o]: Shoulder. [φ]: Very broad peak.

2-2. Measurements

Compounds **3b-i** and **4b-i** synthesised here were identified by ^{1}H-NMR measurements (BRUKER DRX-400) and FT-IR measurements (SHIMADZU FTIR-8400). The phthalocyanine derivatives (**2b-i**) synthesised here were confirmed by MALDI-TOF mass spectra and elemental analyses (Table 1). MALDI- TOF mass spectra were measured using Autoflex III-2S. Elemental analyses were performed using a Perkin-Elmer elemental analyser 2400. Electronic absorption spectra were measured using a Hitachi U-4100 automatic spectrophotometer (Table 2). The phase transition behaviour of **2b-i** was clarified by polarizing microscope observation (Nikon E-600 POL polarization microscope with hot stage consisting of Mettler FP-90 Central Processor) and differential scanning calorimetry (Shimadzu DSC-50). The decomposition temperatures were measured with a Rigaku Thermo plus TG 8120 thermogravimeter. The mesophases were identified using a small angle X-ray diffractometer (Bruker Mac SAXS System) equipped with a hot stage (Mettler FP82HT hot stage, Mettler FP-90 Central Processor).[22] The measuring range of this small angle X-ray diffractometer is from 110 Å to 3.0 Å, and the temperature is variable from rt. to 375^{o}C.

3. RESULTS AND DISCUSSION

3-1. Synthesis

Table 1 summarizes the yields, elemental analysis and TOF-mass spectral results for the phthalocyanine derivatives **2b-i** synthesised here. The electronic absorption spectra are summarized in Table 2. Figure 4 shows a spectrum of the representative derivative **2h**. However, UV-vis spectrum could not be measured for **2b** due to lack of the soluble solvent. Nevertheless, **2b** could be judged from the elemental analysis and the TOF-mass spectrum (Table 1) that it was surely prepared.

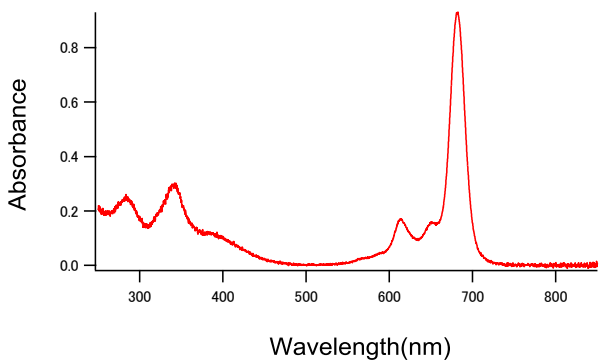

Fig. 4 UV-vis spectrum of (*m*-C_8O)$_8$PcCu (**2h**) in chloroform (3.46×10^{-6} mol/L).

3-2. Phase transition

Table S1 summarizes phase transition behaviours of all the phthalocyanine derivatives (*m*-C_nOPhO)$_8$PcCu (*n* = 1-20: **2a-o**), which were established by using a polarizing optical microscopy (POM), a differential scanning calorimeter (DSC) and a temperature-dependent small angle X-ray diffractometer.

The phase transition behaviours of the previously synthesized derivatives for *n* = 1, 10-20 (**2a**, **2j-o**) have already been reported.[17, 20, 21] Therefore, Table 3 lists only the present derivatives for n = 2-9 (**2b-i**) and the representative previous derivatives for n = 1 (**2a**) and n = 20 (**2o**). The phase transition behaviour of the present derivatives for **2b-i** are described below.

(*m*-C_2OPhO)$_8$PcCu (**2b**) having ethoxy groups (*n* = 2) shows a crystalline phase (K_2) at room temperature (rt) for the freshly prepared virgin sample. When it was heated, it transformed into another crystalline phase (K_3) at 84.2^{o}C and then into K_4 phase at 181.4^{o}C; on further heating, the K_4 phase melted into a rectangular columnar [Col_r(P2m)] mesophase at 274.7^{o}C and it cleared into isotropic liquid (I.L.) at 354.1^{o}C. When the I.L. was cooled, it transformed into the Col_r(P2m) mesophase and then another new crystalline phase (K_1), which was observed only for the non-virgin sample. It is very interesting that each of the short chain derivatives (**2b-d**) for *n* = 2-4 shows only the Col_r(P2m) mesophase, as can been seen from Table 3. The propyloxy derivative (**2e**) for *n* = 5 also shows the same Col_r(P2m) mesophase and an additional monotropic hexagonal ordered columnar (Col_{ho}) mesophase. On the other hand, each of the moderately long chain derivatives (**2f-i**) for *n* = 6-9 shows another type of rectangular columnar [Col_{ro}($P2_1/a$)] mesophase together with Col_{ho} mesophase(s).

It is very noteworthy that the derivative **2h** for *n* = 8 shows an unusual phase transition sequence. As can be seen from the DSC thermograms (Fig. S1) and the photomicrographs of **2h** at various temperatures (Fig. S2), when the virgin sample of **2h** was heated from rt, an unidentifiable X_1 phase transformed into another unidentifiable X_2 phase at 40.4^{o}C; the X_2 phase transformed into Col_{ho1} phase at 83.4^{o}C and then into Col_{ro}($P2_1/a$) phase at 118.9^{o}C. On further heating, it cleared into I.L. at 197.2^{o}C. Thus, the derivative **2h** showed very unusual phase transition sequence from a higher symmetry of Col_h mesophase to a lower symmetry of Col_r mesophase on heating stage. Usually, a lower symmetry of Col_r mesophase transforms into a higher symmetry mesophase on heating stage. As can be seen also from Figs S1 and S2, when the I.L. heated over 205.0^{o}C was cooled down to 200.0^{o}C, it transformed into another hexagonal ordered columnar mesophase of Col_{ho3}; when the Col_{ho3} at 200.0^{o}C was rapidly cooled down to RT, a mixture of supercooled Col_{ho3} and partially resulted Col_{ho2}. Interestingly, the lower symmetry of Col_{ro} mesophase appeared only for the first heating of the virgin sample during such usual observations by DSC and POM. Only when the supercooled Col_{ho3} was held at 165.0^{o}C, the Col_r (bright platelets) phase appeared with Col_{ho2} (dark hexagons), as can be seen from Fig S2.

In contrast with the moderately long chain derivatives (**2f-i**) for *n* = 6-9, each of the longer chain derivatives **2j-o** for *n* = 10-20 shows only Col_h mesophase(s), as can be seen from Table S1 and Table 3.

Thus, the mesomorphism of the present (*m*-C_nOPhO)$_8$PcCu derivatives (**2a-o**) for *n* = 1-20 strongly depends on the alkoxy chain length (*n*): each of the short chain derivatives (**2b-e**) for *n* = 2-5 shows the Col_{ro}(P2m) mesophase; each of the moderately long chain derivatives (**2f-i**) for *n* = 6-9 shows another type of rectangular columnar [Col_{ro}($P2_1/a$)] mesophase together with Col_{ho} mesophase(s); each of the longer chain derivatives **2j-o** for *n* = 10-20 shows Col_h mesophase(s).

Table S2 summarizes small angle X-ray diffraction data of all

the mesophases in the phthalocyanine derivatives **2a-o**. The data of (*m*-C_nOPhO)$_8$PcCu (*n* = 1, 10-20: **2a**, **2j-o**) reported previously [17, 20, 21] are also included for the purpose of comparison.

As can be seen from this table, the phthalocyanine derivatives

Table 3. Phase transition temperatures and enthalpy changes of (*m*-C_nOPhO)$_8$PcCu (n = 1, 2-9 and 20: **2a, 2b-i** and **2o**).

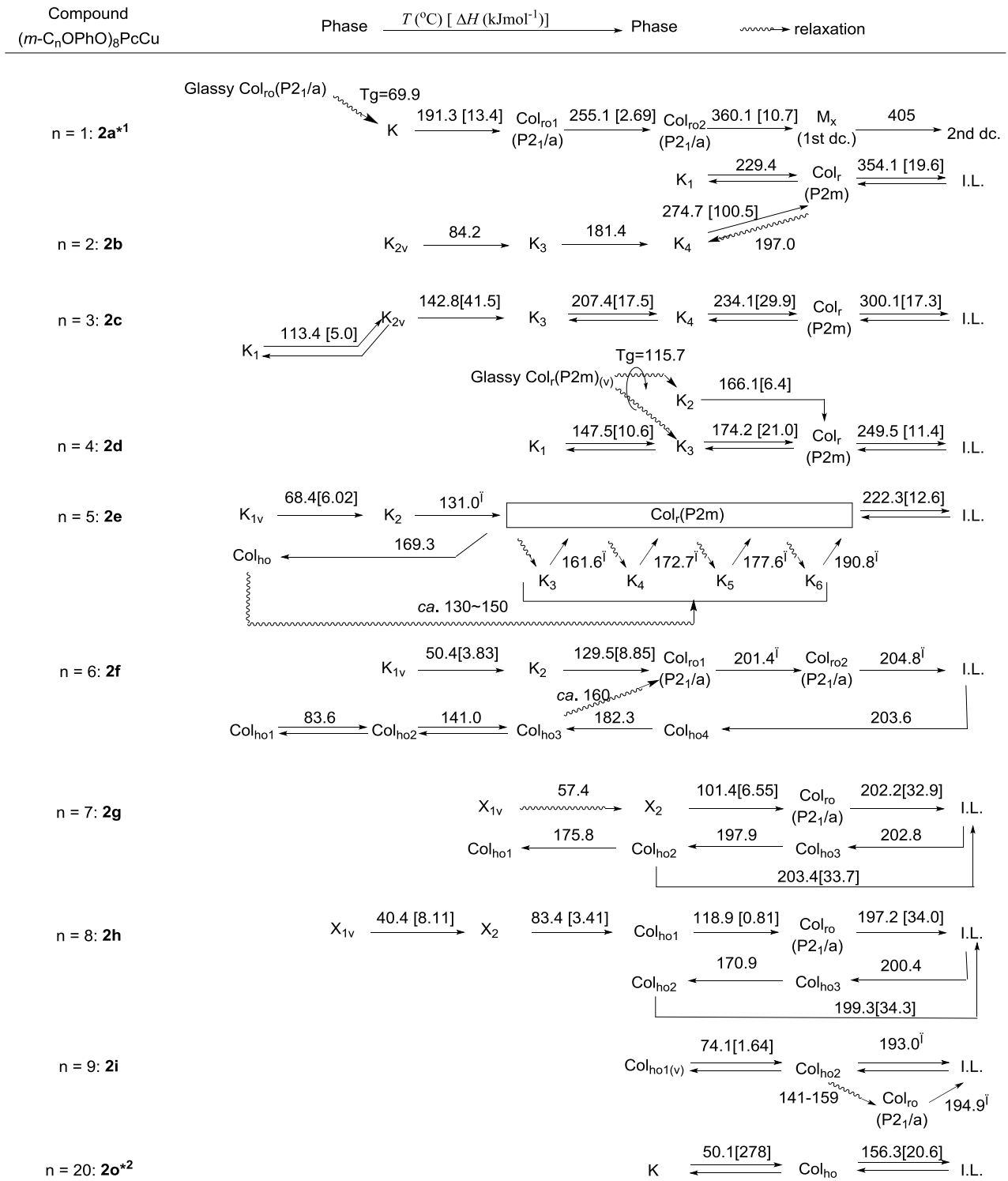

Phase nomenclature: K= crystal, Col_{ro} = rectangular ordered columnar, Col_{ho} = hexagonal ordered columnar mesophase, Col_{hd}=hexagonal disordered columnar mesophase, I.L. = isotropic liquid and v = virgin state. ï: These peaks were so close to calcurate the enthalpy changes. *1: Ref[17], *2: Ref[21].

2b-i (n = 2-9) synthesised in this study could be identified as columnar mesophases from the reflections due to two-dimensional lattices. Although each of the Col_{ho4} phase of (m-$C_6OPhO)_8PcCu$ (**2f**) and the Col_{ho3} phase of (m-$C_7OPhO)_8PcCu$ (**2g**) gave no (110) reflection from the 2D hexagonal lattice, they could be identified as a Col_{ho} phase from Z Value Calculation.[23] When the reflection in the lowest angle is assigned as (1 0 0) of the two-dimensional hexagonal lattice, the Z value becomes 1, which is consistent with the identification as a Col_{ho} mesophase. This identification is also compatible with the textures mentioned below.

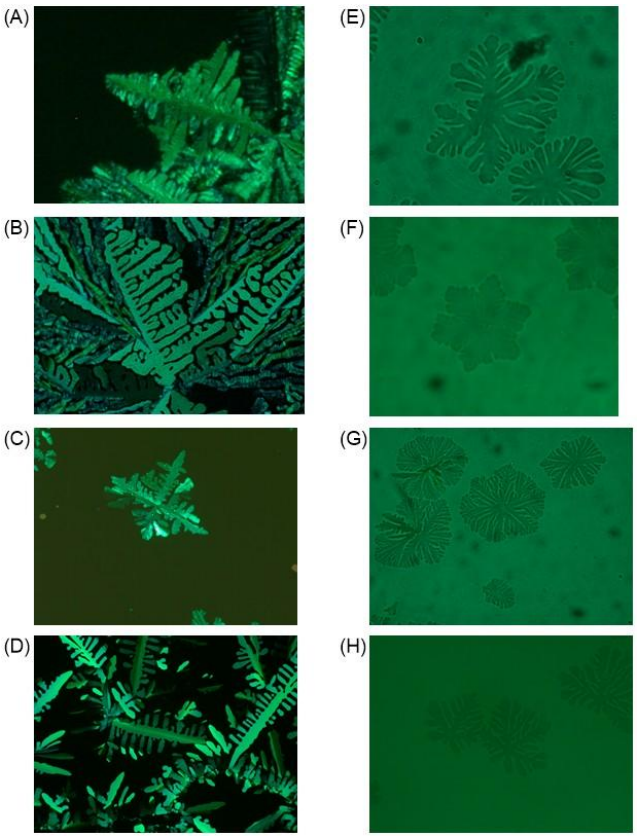

Fig. 5 Photomicrographs of (A) $Col_r(P2m)$ of (m-$C_2OPhO)_8PcCu$ (**2b**) at 340°C; (B) $Col_r(P2m)$ of (m-$C_3OPhO)_8PcCu$ (**2c**) at 280°C; (C) $Col_r(P2m)$ of (m-$C_4OPhO)_8PcCu$ (**2d**) at 245°C; (D) $Col_r(P2m)$ of (m-$C_5OPhO)_8PcCu$ (**2e**) at 200°C; (E) Col_{ho4} of (m-$C_6OPhO)_8PcCu$ (**2f**) at 200°C; (F) Col_{ho3} of (m-$C_7OPhO)_8PcCu$ (**2g**) at 200°C; (G) Col_{ho3} of (m-$C_8OPhO)_8PcCu$ (**2h**) at 199.7°C; (H) Col_{ho2} of (m-$C_9OPhO)_8PcCu$ (**2i**) at 196.5°C.

Figure 5 shows the photomicrographs of the $Col_{ro}(P2m)$ phases of (m-$C_nOPhO)_8PcCu$ for n = 2-5 (**2b-e**) and the Col_{ho} phases of (m-$C_nOPhO)_8PcCu$ for n = 6-9 (**2f-i**). As can be seen from these photomicrographs, each of **2b-e** shows the dendritic textures characteristic to a Col_r phase, and each of **2f-i** shows the dendritic textures characteristic to a Col_h phase having a C_6 symmetry. Furthermore, they showed no birefringence resulted from homeotropic alignment. Thus, these $Col_{ro}(P2m)$ of **2b-e** and Col_{ho} phases of **2f-i** could be identified from the XRD data and characteristic textures.

In Figure 6, the phase transition temperatures are plotted against the carbon number (n) in the alkoxy chain. As can be seen from this figure, the derivative **2a** (n = 1) shows $Col_{ro1}(P2_1/a)$ and $Col_{ro2}(P2_1/a)$ phases, and each of the derivatives **2b-d** (n = 2-4) shows a $Col_r(P2m)$ phase. Therefore, the derivatives **2a-d** (n = 1-4) tend to show only the rectangular columnar (Col_r) mesophase(s). On the other hand, the derivative **2e** (n = 5) shows an enantiotropic $Col_r(P2m)$ mesophase and a monotropic Col_{ho} phase. Interestingly, the derivatives **2f-h** (n = 6-8) tend to show enantiotropic Col_{ho} phase(s) and $Col_{ro}(P2_1/a)$ phase(s). As can be seen from Table 3, the $Col_{ro}(P2_1/a)$ phase(s) in the derivatives **2f-h** (n = 6-8) appeared almost only for the freshly prepared virgin sample. Once it cleared into IL, the non-virgin sample gave only Col_{ho} mesophases. This phenomenon can be rationally explained by using Gibbs free energy vs. temperature (G-T) diagram.[24] For a representative derivative **2h** (n = 8), the G-T diagram is illustrated in Figure S3. Although the derivatives **2i** (n = 9) also shows the Col_{ho} and $Col_{ro}(P2_1/a)$ phase(s), the $Col_{ro}(P2_1/a)$ phase was only observed for relaxation from the Col_{ho} phase. On the other hand, each of the derivatives **2j-o** (n = 10-20) shows only enantiotropic Col_h phase(s), without any rectangular columnar (Col_r) phases. Thus, the phase transition behaviour critically changes, between n = 1and 2, between n = 5 and 6, and between n = 9 and 10, as indicated dotted lines in

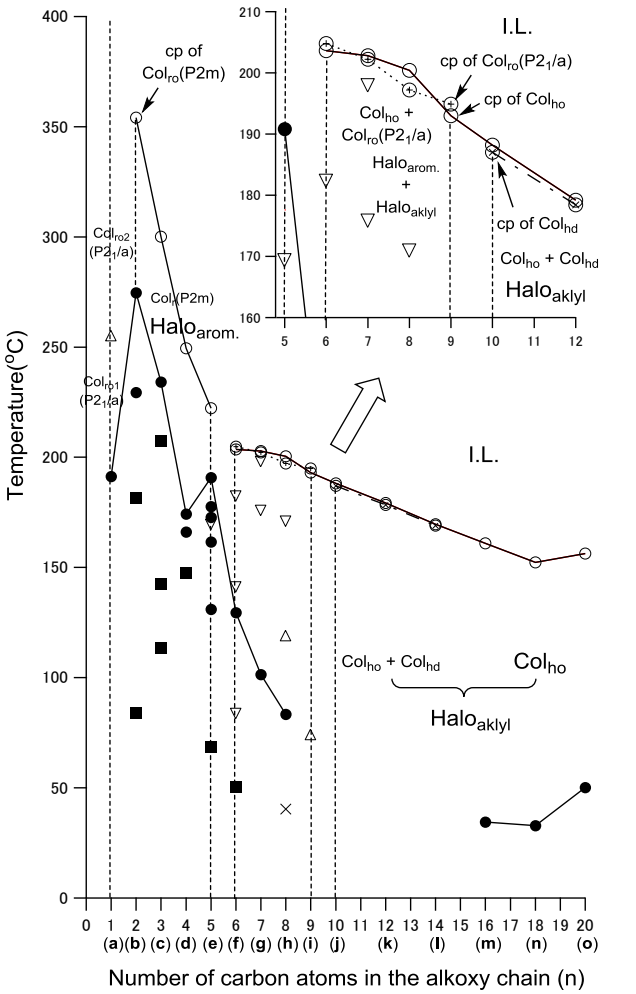

Fig. 6 Phase transition temperatures versus number of carbon atoms in the alkoxy chain (n) for (m-$C_nOPhO)_8PcCu$ (n = 1~20: **2a-o**).

Figure 6. For n = 1, the derivative decomposes at higher temperatures. Excluding this derivative, all the other derivatives can be classified into three groups: the short chain derivatives (**2b-e**) for *n* = 2-5; the moderately long chain derivatives (**2f-i**) for *n* = 6-9; the longer chain derivatives **2j-o** for *n* = 10-20.

At these group boundaries between n = 5 and 6 and between n = 9 and 10, the driving force of mesomorphism may be changed. We predicted from this figure that the driving force of mesomorphism might be attributable to rotation or flip-flop of only the bulky aromatic substituents for *n* = 2-5, but melting of only the alkyl chains for *n* = 10-20. In between for n = 6-9, both of rotation of the bulky groups and melting of the longer alkyl groups may originate their mesomorphism. In order to confirm this hypothesis, we have carried out further detailed temperature-dependent X-ray diffraction measurements.

3-3. Temperature-dependent X-ray diffraction measurements

For the detailed temperature-dependent X-ray diffraction measurements, we chose three representative derivatives from each of the three groups: **2b** (*n* = 2) for *n* = 2-5, **2h** (*n* = 8) for *n* = 6-9, and **2o** (*n* = 20) for *n* = 10-20.

Figure 7 shows the X-ray diffraction patterns of the mesophases of **2b** (*n* = 2) at 290°C and **2o** (*n* = 20) at 100°C. As can be seen from Figure 7(1), **2b** (*n* = 2) shows a halo at 2θ ≅ 17° (about 5.2 Å) (**Halo$_{arom.}$**: denoted as #1) in the Col$_r$(P2m) mesophase, which is due to flip-flop of the bulky aromatic substituents. On the other hand, as can be seen from Figure 7(2), **2o** (*n* = 20) shows a halo at 2θ ≅ 18.5° (about 4.6 Å) (**Halo$_{alkyl}$**: denoted as #2) in the Col$_{ho}$ mesophase, which is due to the molten alkyl chains. The **Halo$_{arom.}$** of **2b** (*n* = 2) in Figure 7(1) could not be observed in the X-ray diffraction pattern of **2o** (*n* = 20) in Figure 7(2), whereas the **Halo$_{alkyl}$** of **2o** (*n* = 20) in Figure 7(2) could not be observed in the X-ray diffraction pattern of **2b** (*n* = 2) in Figure 7(1). That means that the mesomorphism of **2b** (*n* = 2) is induced only by the driving force originated from flip-flop of the bulky substituents, but that the mesomorphism of **2o** (*n* = 20) is induced only by the driving force originated from the molten alkyl chains.

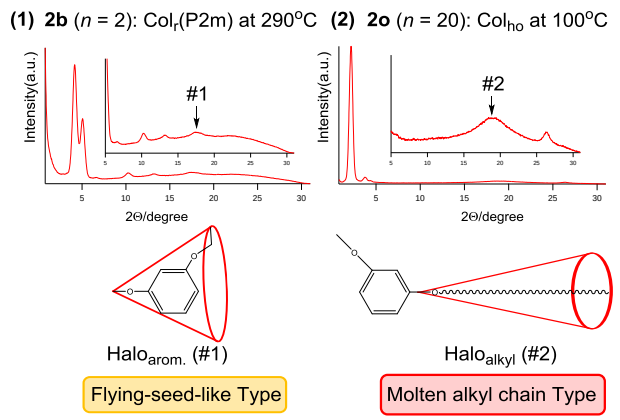

Fig. 7 Two different types of halos in the X-ray diffraction patterns of (1) (*m*-C$_2$OPhO)$_8$PcCu (**2b**) at 290°C and (2) (*m*-C$_{20}$OPhO)$_8$PcCu (**2o**) at 100°C.

In Figure 8 are plotted the spacing values of **Halo$_{arom.}$** (#1) of **2b** (*n* = 2) and **Halo$_{alkyl}$** (#2) of **2o** (*n* = 20) against temperature. As can be seen from this figure, both **Halo$_{arom.}$** (#1) and **Halo$_{alkyl}$** (#2) show their abrupt value jumps at the phase transition temperatures from crystal (K) to columnar (Col) mesophase. It is noteworthy that the value of **Halo$_{arom.}$** (#1) jumps to 5.2 Å at the K-Col phase transition temperature, 274.7°C, whereas the **Halo$_{alkyl}$** (#2) jumps to 4.6 Å at the K-Col phase transition temperature, 53.7°C. Furthermore, the spacing value of **Halo$_{alkyl}$** (#2) gradually increases from 4.6 Å to 4.8 Å with elevating the temperature to 140°C. Thus, the spacing values of **Halo$_{arom.}$** (#1) and **Halo$_{alkyl}$** (#2) are located at *ca.* 5.2 Å and 4.6-4.8 Å, respectively. Therefore, we can distinguish **Halo$_{arom.}$** (#1) and **Halo$_{alkyl}$** (#2) from their spacing values.

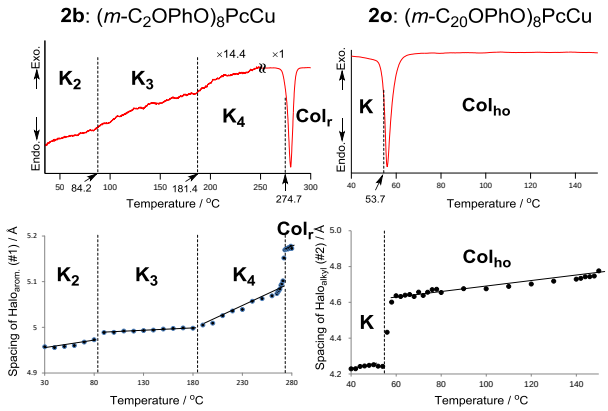

Fig. 8 Thermal dependence of the spacing of halos due to the flip-flopping aromatic groups (ca. 5.2 Å) of (*m*-C$_2$OPhO)$_8$PcCu (**2b**) and the molten alkyl groups (*ca.* 4.6~4.8 Å) of (*m*-C$_{20}$OPhO)$_8$PcCu (**2o**).

Figure 9 shows the X-ray diffraction patterns for the moderately long chain derivative 2h (n = 8) showing an unusual phase transition sequence from the Col$_{ho}$ phase to the Col$_{ro}$(P2$_1$/a) phase on heating stage. This is completely reverse to the normal phase transition sequence. Usually, a phase transition occurs from a lower symmetry of Col$_{ro}$ mesophase to a higher symmetry of Col$_{ho}$ mesophase. This reverse sequence may be attributed to both flip-flop of the bulky aromatic substituents and melting of the

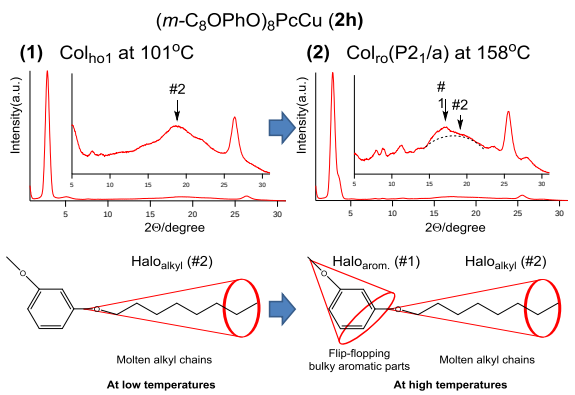

Fig. 9 X-ray diffraction patterns of (*m*-C$_8$OPhO)$_8$PcCu (**2h**) at (1)101°C and (2)158°C.

alkyl chains. As can be seen from the X-ray diffraction patterns of Col$_{ho1}$ phase shown in Figure 9(1), **Halo$_{alkyl}$** (#2) only appears. On the other hand, as can been seen from the X-ray diffraction patterns of Col$_{ro}$(P2$_1$/a) phase shown in Figure 9(2), **Halo$_{arom.}$** (#1) appears as a large peak covered on the **Halo$_{alkyl}$** (#2). Hence, in the lower temperature region, the alkyl chain only melts to

show the Col_{ho1} phase, but in the higher temperature region, the bulky aromatic substituents also flip-flop to show the $Col_{ro}(P2_1/a)$ phase.

To further confirm this phenomenon, we carried out fine X-ray diffraction measurements by changing the temperature in small increments. Figure 10 shows the X-ray diffraction patterns of (m-C_8OPhO)$_8$PcCu (**2h**) measured in an angle region from 5 to 31 degree at 32 different temperatures. As can be seen from this figure, the halo due to the molten alkyl chains (**Halo$_{alkyl}$**: #2) appeared for X_2 phase (blue lines) and Col_{ho1} phases (green lines), whereas the halo due to the flip-flopping aromatic groups (**Halo$_{arom.}$**: #1) appeared only for Col_{ro} phase (red lines). Apparently, the halo suddenly shifted to lower angle at the phase transition from Col_{ho1} phase to Col_{ro} phase.

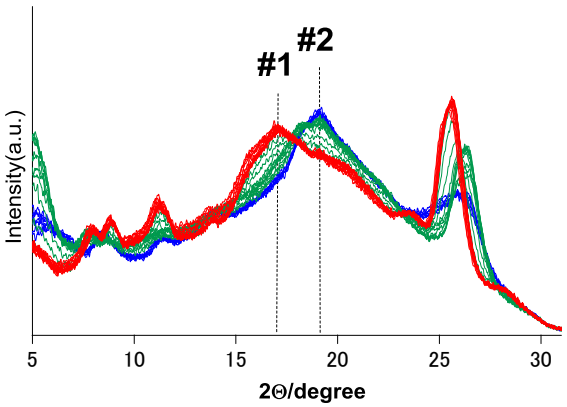

Fig. 10 Temperature-dependent X-ray diffraction patterns of (m-C_8OPhO)$_8$PcCu (**2h**) in the rage of 2Θ = 5~31. Blue lines: X_2 phase at 70, 75, 77, 78, 79, 80 and 81 °C. Green lines: Col_{ho1} phase at 87, 88, 90, 100, 105, 110, 113, 114, 115, 116, 117 and 118 °C. Red lines: Col_{ro} phase at 119, 120, 121, 122, 123, 125, 130, 140, 150, 160, 170, 180 and 190 °C. #1: **Halo$_{arom.}$** = halo due to the flip-flopping aromatic groups (*ca.* 5.2 Å). #2: **Halo$_{alkyl}$** = halo due to the molten alkyl chains (*ca.* 4.6~4.8 Å).

In Figure 11, all the spacing values of **Halo$_{alkyl}$** (#2) and **Halo$_{arom.}$** (#1) of **2h** are plotted against temperature on heating stage. As can be seen from this figure, the spacing values of #2 at about 4.8 Å in the lower temperature region suddenly jumps to the spacing value of #1 at about 5.2 Å in the lower temperature region, just at the phase transition from the Col_{ho1} mesophase to the $Col_{ro}(P2_1/a)$ mesophase at 118.9°C. Thus, it could be confirmed that the Col_{ho} phase in the lower temperature region is originated by melting of the alkyl chains, and that the $Col_{ro}(P2_1/a)$ phase in the higher temperature region is originated by flip-flop of the bulky aromatic substituents. Such a stepwise melting of these substituents may result in this present reverse phase transition sequence from a higher symmetry of Col_h mesophase to a lower symmetry of Col_r mesophase for the moderately long chain derivative **2h** (n = 8). Furthermore, this mesogen is the first example switching from long alkyl chain type to flying-seed-like type in a discotic liquid crystal, so far as we know.

4. CONCLUSION

In this study, a series of phthalocyanine derivatives (m-C_nOPhO)$_8$PcCu (n = 1-20: **2a-o**) were prepared to investigate

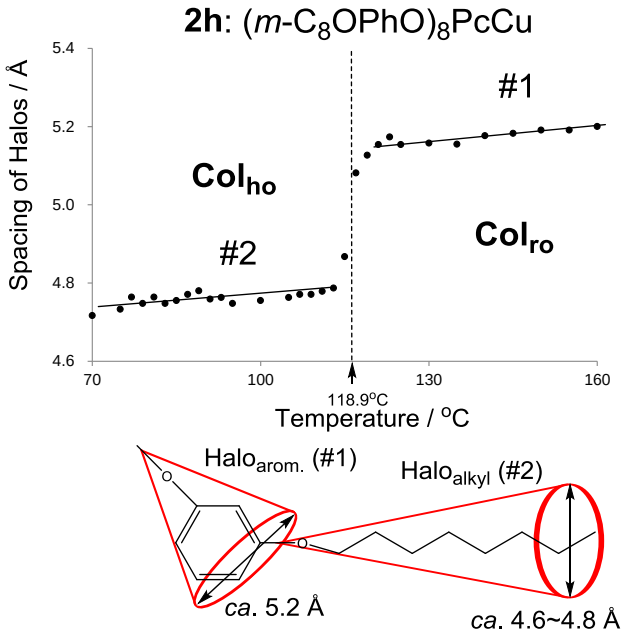

Fig. 11 Thermal dependence of the spacing of halos due to the molten alkyl groups (ca. 4.6~4.8 Å) and the flip-flopping aromatic groups (*ca.* 5.2 Å) of (m-C_8OPhO)$_8$PcCu (**2h**).

the mesomorphism. The mesomorphism of the present (m-C_nOPhO)$_8$PcCu derivatives (n = 1-20: **2a-o**) strongly depends on the alkoxy chain length (n). The mesomorphism of the short chain-substituted derivatives **2a-e** for n = 1~5 is flying-seed-like type induced by flip-flop of the peripheral bulky substituents, whereas the mesomorphism of the long chain-substituted derivatives **2j-o** for n = 10~20 is conventional molten alkyl chain type induced by melting of the long alkyl chains. The moderately long chain derivatives (**2f-i**) for n = 6-9 in between show both types of mesophases. The temperature-dependent small angle X-ray diffraction studies revealed that a halo denoted as **Halo$_{arom.}$** appeared in the short chain derivatives (**2b-e**) for n = 2-5 at d ≅ 5.2 Å due to flip-flop of the bulky aromatic substituents, and that another halo denoted as **Halo$_{alkyl}$** appeared in the longer chain derivatives **2j-o** for n = 10-20 at d ≅ 4.6-4.8 Å due to melting of the long alkyl chains. Therefore, we can distinguish the type of mesophase from **Halo$_{arom.}$** and **Halo$_{alkyl}$**. Very interestingly, the moderately long chain derivative (m-C_8OPhO)$_8$PcCu (**2h**) gave the **Halo$_{alkyl}$** in the lower temperature mesophase of Col_{ho} at about 4.8 Å, and the **Halo$_{arom}$** in the higher temperature mesophase of $Col_{ro}(P2_1/a)$ phase at about 5.2 Å. This means that melting of the alkyl chains induces the Col_{ho1} phase in the lower temperature region, but that flip-flop of the bulky aromatic substituents induces the $Col_{ro}(P2_1/a)$ phase in the higher temperature region. Furthermore, this unusual reverse phase transition sequence from a higher symmetry of Col_h mesophase to a lower symmetry of Col_r mesophase is attributable to the stepwise melting of the substituents. To our best knowledge, this mesogen (**2h**) is the first example switching from molten alkyl chain type to flying-seed-like type in a discotic liquid crystal.

Notes

[a]*Smart Material Science and Technology, Interdisciplinary Graduate School of Science and Technology, Shinshu University, 1-15-1 Tokida,*

Ueda, 386-8567, Japan. E-mail: ko52517@shinshu-u.ac.jp; Fax: +81-268-21-5492; Tel: +81-268-21-5492
[b]Comprehensive Analysis Centre for Science, Saitama University, 255 Shimo-okubo, Sakura-ku, Saitama 338-8570, Japan. E-mail: yasutake@apc.saitama-u.ac.jp; Tel. +81-48-858-3671

References

1 H. Keller, *Mol. Cryst. Liq. Cryst.* 1973, **21**, 1-48; V. Vill, *Condensed Matter News* 1992, **1**, 25-28.
2 Database of liquid crystalline compounds for personal computer, *LiqCryst Version 5*, ed. Vill V., LCI Publisher and Fujitsu Kyushu Systems Limited, 2010.
3 D. Vorländer, *Ber. Dtsch. Chem. Ges*., 1911, **43**, 3120–3125.
4 D. Demus, H. Sackmann, and K. Seibert, *Wiss. Z. Univ. Halle, Math.-Nat. R.* 1970, **19**, 47-62.
5 P. Ferloni, M. Sanesi, P. L. Tonelli and P. Franzosini, *Z. Naturforsch.* 1978, **33a**, 240-242.
6 M. Sanesi, P. Ferloni, G. Spinolo and P. L. Tonelli, *Z. Naturforsch.* 1978, **33a**, 386-388.
7 R. van Deun, J. Ramaekers, P. Nockemann, K. van Hecke, L. van Meervelt and K. Binnemans, *Eur. J. Inorg. Chem.*, 2005, 563-571.
8 K. Ohta, T. Shibuya and M. Ando, *J. Mater. Chem.*, 2006, **16**, 3635-3639.
9 S. Basurto, S. Garcia, A. G. Neo, T. Torroba, C. F. Marcos, D. Miguel, J. Barbera, M. B. Ros and M. R. de la Fuente, *Chem. Eur. J.*, 2005, **11**, 5362-5376.
10 M. Shimizu, M. Nata, K. Watanabe, T. Hiyama and S. Ujiie, *Mol. Cryst. Liq. Cryst.*, 2005, **441**, 237-241.
11 M. Shimizu, M. Nata, K. Mochida, T. Hiyama, S. Ujiie, M. Yoshio and T. Kato, *Angew. Chem. Int. Ed.*, 2007, **46**, 3055-3058.
12 N. Usol'tseva, V. Bykova, G. Ananjeva and N. Zharnikova, *Mol. Cryst. Liq. Cryst.* 2004, **411**, 1371-1378.
13 N. Zharnikova, N. Usol'tseva, E. Kudrik and M. Theakkat, *J. Mater. Chem.*, 2009, **19**, 3161-3167.
14 Y. Takagi, K. Ohta, S. Shimosugi, T. Fujii and E. Itoh, *J. Mater. Chem*., 2012, **22**, 14418-14425.
15 A. Hachisuga, M. Yoshioka, K. Ohta and T. Itaya, *J. Mater. Chem.*, 2013, **1**, 5315-5321.
16 A. Ishikawa, K. Ohta and M. Yasutake, *J. Porphyrins Phthalocyanines*, 2015, **19**, 639-650.
17 M. Yoshioka, K. Ohta and M. Yasutake, *RSC Advances*, 2015, **5**, 13828-13839.
18 A. Watarai, K. Ohta and M. Yasutake, *J. Porphyrins Phthalocyanines*, 2016, **20**, 822-832.
19 K. Ohta, K. Adachi and M. Yasutake, *J. Porphyrins Phthalocyanines*, 2017; **21**: 48-58.
20 M. Ichihara, A. Suzuki, K. Hatsusaka and K. Ohta, *J. Porphyrins Phthalocyanines*, 2007, **11**, 503.
21 H. Sato, K. Igarashi, Y. Yama, M. Ichihara, E. Itoh and K. Ohta, *J. Porphyrins Phthalocyanines*, 2012, **16**, 1148-1158.
22 L. Tauchi, T. Nakagaki, M. Shimizu, E. Itoh, M. Yasutake and K. Ohta, *J. Porphyrins Phthalocyanines*, 2013, **17**, 264-282.
23 K. Ohta, *"Dimensionality and Hierarchy of Liquid Crystalline Phases: X-ray Structural Analysis of the Dimensional Assemblies"*, Shinshu University Institutional Repository, submitted on 11 May, 2013; http://hdl.handle.net/10091/17016; K. Ohta, "*Identification of discotic mesophases by X-ray structure analysis*," in "*Introduction to Experiments in Liquid Crystal Science (Ekisho Kagaku Jikken Nyumon [in Japanese])*," ed., Japanese Liquid Crystal Society, Chapter 2-(3), pp. 11-21, Sigma Shuppan, Tokyo, 2007; ISBN-13: 978-4915666490.
24 G-T diagram: *e.g.*, see Fig. 1 in the following paper: H. Sato, Y. Sakagami, E. Itoh and K. Ohta, *J. Porphyrins Phthalocyanines*, 2012, **16**, 1209–1216. This G-T diagram can rationally explain the mesophase appearance different between the virgin sample and the non-virgin sample.